Line radiation events induced by very low frequency transmitters observed by the DEMETER spacecraft — Source link ↗

František Němec, K. Čížek, Michel Parrot, Ondrej Santolik ...+2 more authors

Institutions: Charles University in Prague, Centre national de la recherche scientifique, Academy of Sciences of the Czech Republic

Related papers:

- Unusually high frequency natural VLF radio emissions observed during daytime in Northern Finland

- Frequency-time behavior of artificially stimulated VLF emissions

- A new type of daytime high-frequency VLF emissions at auroral latitudes ("bird emissions")

- New high-frequency (7–12 kHz) quasi-periodic VLF emissions observed on the ground at L ~ 5.5

- Magnetospheric VLF line radiation observed at Halley, Antarctica

Line radiation events induced by very low frequency transmitters observed by the DEMETER spacecraft

F. Němec, K. Čížek, Michel Parrot, O. Santolík, J. Záhlava

Correspondence to:
F. Nemec,
frantisek.nemec@gmail.com

Line radiation events induced by very low frequency transmitters observed by the DEMETER spacecraft

F. Němec[1] , **K. Čížek**[1] , **M. Parrot**[2] , **O. Santolík**[1,3] , and **J. Záhlava**[1]

[1]Faculty of Mathematics and Physics, Charles University, Prague, Czech Republic, [2]LPC2E/CNRS, Orléans, France, [3]Institute of Atmospheric Physics, Czech Academy of Sciences, Prague, Czech Republic

Abstract Electromagnetic wave data measured by the low-altitude Detection of Electro-Magnetic Emissions Transmitted from Earthquake Regions (DEMETER) spacecraft sometimes exhibit intense emissions at discrete, harmonically spaced frequencies. We present a comprehensive analysis of this type of phenomenon, and we demonstrate that it is caused by very low frequency (VLF) transmitters in Europe. All available data were investigated for a possible presence of the events. Altogether, 87 events were identified, occurring exclusively during the nighttime. The occurrence of the events does not show any clear relation to the *AE* and *Dst* geomagnetic activity indices. The events are clearly localized, occurring either close to Great Britain or in the vicinity of its geomagnetically conjugated region. The frequency spectra of the events typically consist of up to four spectral peaks at multiples of about 1.3 kHz. Additional weaker spectral peaks at frequencies of about 1.9 kHz and 3.2 kHz are occasionally present. The events observed in the Northern Hemisphere tend to have larger-frequency bandwidths than the events observed in the Southern Hemisphere. The occurrence of these events is correlated with the simultaneous detection of signals from VLF transmitters. A bicoherence analysis is employed to demonstrate that wave-wave coupling takes place. Finally, it is shown that the occurrence of the events is associated with a significantly increased precipitation of energetic electrons in a wide range of energies.

1. Introduction

A careful investigation of very low frequency (VLF) electromagnetic wave data measured by the low-altitude Detection of Electro-Magnetic Emissions Transmitted from Earthquake Regions (DEMETER) spacecraft over the course of its mission (2004–2010) has revealed many unexpected wave phenomena [*Parrot et al.*, 2015]. Among these, there is a particular group of events that, when represented in a traditional form of frequency-time spectrograms, has a form of several distinct nearly horizontal lines. These have been extensively studied in the past. It was shown that some of them, which have the frequency spacing corresponding to multiples of 50 or 60 Hz, are related to electromagnetic radiation from electric power systems on the ground [*Němec et al.*, 2006, 2007, 2008; *Dudkin et al.*, 2015; *Korepanov et al.*, 2015; *Němec et al.*, 2015]. Such events are usually called power line harmonic radiation (PLHR). The remaining events, whose frequency spacing does not correspond to the base frequency of electric power systems, are usually called magnetospheric line radiation (MLR). Although their basic properties are rather well known [*Němec et al.*, 2009, 2012; *Bezděková et al.*, 2015], their generation mechanism remains unclear. Such emissions were, nevertheless, observed also on the ground [*Rodger et al.*, 1999, 2000a], and their origin is likely natural [*Rodger et al.*, 2000b]. Both PLHR and MLR events are eventually able to trigger new types of emissions [*Nunn et al.*, 1999; *Parrot and Němec*, 2009; *Němec et al.*, 2010; *Parrot et al.*, 2014] and possibly affect the VLF wave intensity in the inner magnetosphere [*Park and Helliwell*, 1978; *Park and Miller*, 1979; *Park and Helliwell*, 1981; *Molchanov et al.*, 1991; *Parrot*, 1991].

Apart from the unintentional radiation from power lines, the inner magnetosphere is invaded by a significant number of narrowband artificial VLF signals coming from powerful military VLF transmitters [*Starks et al.*, 2008; *Cohen and Inan*, 2012]. Although these signals are, particularly during the daytime, attenuated by their propagation through the ionosphere [*Tao et al.*, 2010; *Cohen et al.*, 2012; *Graf et al.*, 2013], and eventually scattered by density irregularities [*Bell et al.*, 2008; *Foust et al.*, 2010; *Shao et al.*, 2012], they are readily detectable by satellites both above the source and in the magnetically conjugated regions [*Cohen and Inan*, 2012]. Moreover, they

can induce a significant precipitation of energetic electrons at resonant energies [*Inan et al.*, 2007; *Gamble et al.*, 2008; *Kulkarni et al.*, 2008; *Sauvaud et al.*, 2008; *Graf et al.*, 2009], and they might be possibly responsible for the so-called impenetrable barrier recently reported in radial profiles of relativistic electrons in the outer radiation belt [*Baker et al.*, 2014; *Foster et al.*, 2016].

In the present study, we focus on the analysis of exceptional electromagnetic wave events reported by *Parrot et al.* [2015] in the DEMETER spacecraft data. Although they could be technically classified as MLR, their frequency-time structure is somewhat different. Specifically, they have a clearly defined harmonic structure with frequencies constant in time, and their apparent time duration (spatial extent) is generally rather low as compared to typical MLR events. We indeed demonstrate that their properties are rather unique and that their generation can be linked to VLF transmitter signals and subsequent wave-wave interactions taking place. We therefore show that these transmitter induced line radiation (TILR) events constitute a separate class of wave phenomena.

The DEMETER spacecraft, its instrumentation relevant for the performed analysis, and the used data set are described in section 2. The obtained results are presented in section 3, and they are discussed in section 4. Finally, section 5 presents a brief summary of the main results.

2. Data Set

DEMETER was a French low-altitude spacecraft operating between 2004 and 2010. During about 6.5 years of the mission, it collected a large amount of scientific data at geomagnetic latitudes lower than approximately 65°. The orbit of the spacecraft was circular, with the altitude of about 700 km. Moreover, the orbit was nearly Sun synchronous; i.e., the satellite was always located either close to the local noon (approximately 10:30 LT) or close to the local midnight (approximately 22:30 LT).

Among various measurements performed, we are particularly interested in electromagnetic wave measurements in the VLF range. Although both electric [*Berthelier et al.*, 2006] and magnetic [*Parrot et al.*, 2006] field measurements were performed, the magnetic field data suffer from onboard interferences at frequencies up to about 10 kHz, and thus, only electric field data will be used in the present study. Two principal types of data were collected. In the continuously active Survey mode, the data consist of onboard calculated frequency-time spectrograms of one electric field component up to 20 kHz. The frequency resolution was about 20 Hz, and the time resolution was about 2 s. In the Burst mode, which was active only during specific (usually a few minutes long) time intervals, high-resolution data were collected. These consisted of a waveform of one electric field component with the sampling frequency of 40 kHz. A low-pass filtering was applied before the data sampling. The frequency response of the filter was flat up to 17.4 kHz, with the slope at higher frequencies of about −12 dB/octave [*Parrot et al.*, 2006]. This allows strong signals with frequencies above the Nyquist frequency to be detected in the DEMETER VLF data due to the aliasing.

Apart from the electromagnetic wave instruments, DEMETER was also equipped by a solid-state detector of energetic electrons [*Sauvaud et al.*, 2006]. This provided measurements of electron fluxes close to the loss cone. The time resolution was 4 s, and there were 128 equally spaced energy channels in the energy range from 64 keV to 2.35 MeV.

Two examples of TILR events are shown in Figure 1 using frequency-time spectrograms of power spectral density of electric field fluctuations covering all the analyzed frequency range. The event shown in Figure 1a was measured on 9 February 2010 between about 21:18 UT and 21:19 UT, when the spacecraft was located in the Northern Hemisphere. The event shown in Figure 1b was measured on 13 August 2004 between about 21:39 UT and 21:41 UT, when the spacecraft was located in the Southern Hemisphere. Both these TILR events were measured during the nighttime. They consist of several harmonically spaced spectral lines at frequencies spanning from 0 up to 5 kHz. The intense horizontal lines at frequencies higher than about 16 kHz are electromagnetic signals from VLF transmitters. It can be seen that at the times of the events, the intensity of these signals is increased and their frequency bandwidths broaden as compared to nearby time intervals. Moreover, it is noticeable that the frequency bandwidth of the lines forming the events below 5 kHz is significantly larger for the event in Figure 1a than for the event in Figure 1b. The emissions with vertical frequency-time signatures are electromagnetic waves generated by lightning activity (0+ whistlers), and they are of no interest for the performed analysis.
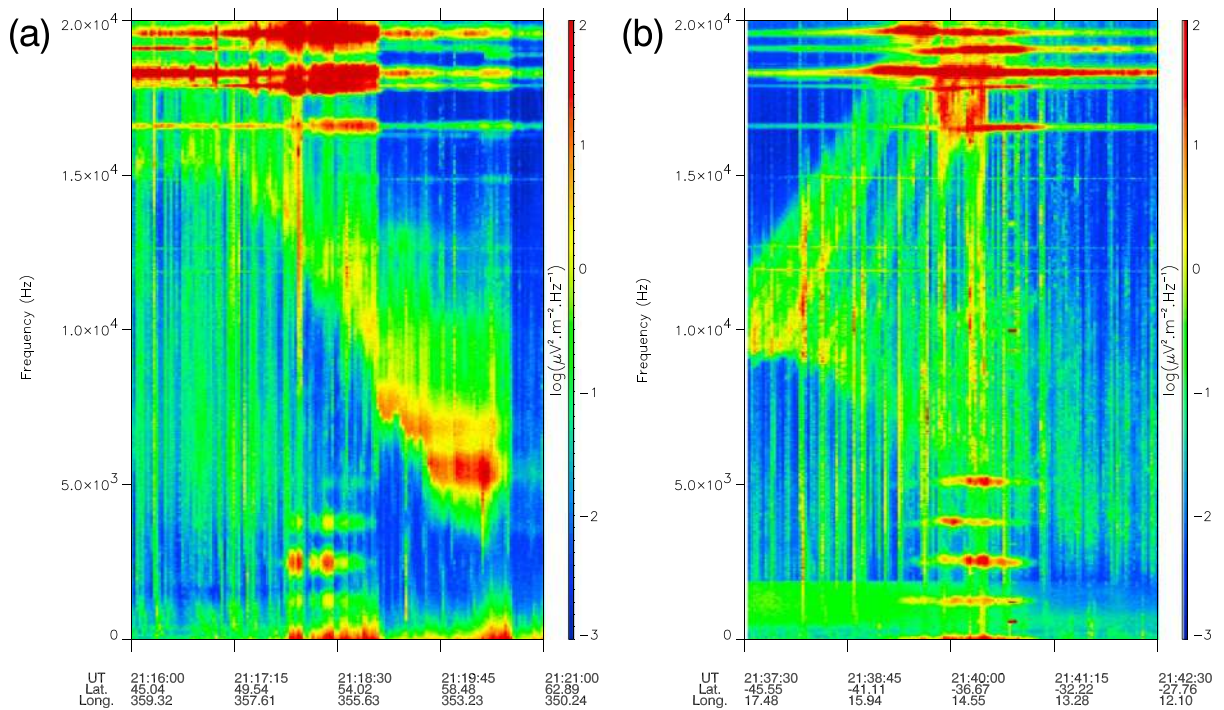
Figure 1. a) Frequency-time spectrogram of power spectral density of electric field fluctuations corresponding to an event observed in the Northern Hemisphere. The data were obtained on 9 February 2010 between 21:16 UT and 21:21 UT. The event consisting of several broadband horizontal intense lines is observed between about 21:18 UT and 21:19 UT at frequencies up to about 5 kHz. (b) Frequency-time spectrogram of power spectral density of electric field fluctuations corresponding to an event observed in the Southern Hemisphere. The data were obtained on 13 August 2004 between 21:37:30 UT and 21:42:30 UT. The event consisting of five intense horizontal lines significantly narrower than in Figure 1a is observed between about 21:39 UT and 21:41 UT at frequencies up to about 5 kHz.

We note that although single-point measurements do not in principle allow us to distinguish between spatial and temporal variations, the analysis hereinafter strongly suggests that the observed short time durations of the events are a consequence of their limited spatial extent and a moving satellite. The real-time durations of the events may be substantially larger than the observed time durations.

We have visually inspected all Survey mode VLF data measured by the DEMETER spacecraft for the presence of the TILR events. For this purpose, a frequency-time spectrogram of each DEMETER half-orbit (about 35 min) spanning from 0 to 20 kHz was plotted, and the presence/absence of the events was manually determined. If present, the beginning and ending times of the event were marked. Altogether, 87 events were identified.
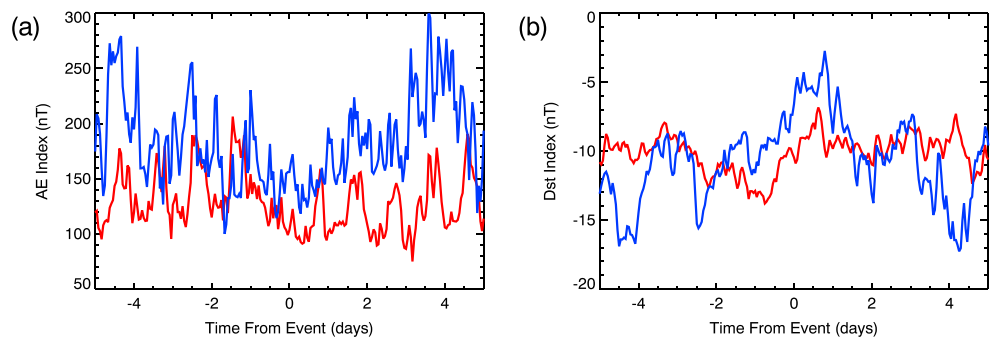
Figure 2. Superposed epoch analysis of the variation of geomagnetic indices around the times of all 87 TILR events. (a) Mean value of *AE* index as a function of the time relative to the times of the events. The results obtained for the events observed in the Northern Hemisphere are shown by the red curve, and the results obtained for the events observed in the Southern Hemisphere are shown by the blue curve. (b) The same as Figure 2a but for mean value of *Dst* index.
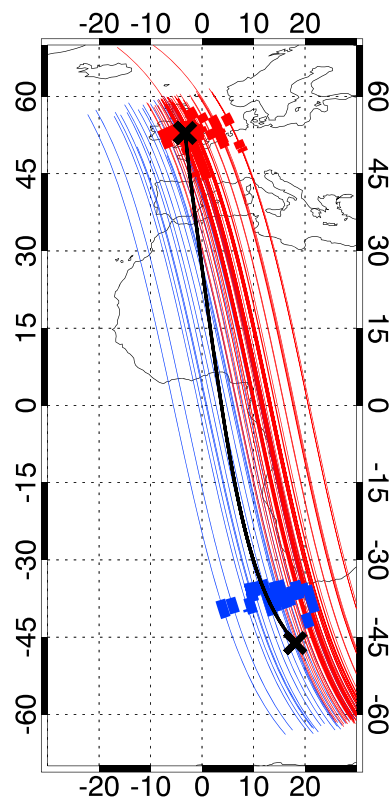
Figure 3. Geographic map of the spacecraft locations at the times when the events were observed. The thin red and blue curves show the projections of the spacecraft half-orbits when events were observed in the Northern Hemisphere and in the Southern Hemispheres, respectively. The spacecraft locations at the times when the events were observed in the Northern and Southern Hemispheres are shown by the thick red and blue curves, respectively. The thick black cross in the Northern Hemisphere marks the location of the GQD/GBZ VLF transmitter in Anthorn, Great Britain ($L \approx 2.40$). The thick black cross in the Southern Hemisphere shows the location of the geomagnetically conjugated point. The black curve shows the projection of the corresponding magnetic field line.

It is found that they occur exclusively during the nighttime, with no event identified during the daytime. The resulting list of events is the starting point of the presented analysis.

3. Results

It is of interest to investigate whether the TILR event occurrence is related to some specific geomagnetic conditions, e.g., if they occur preferentially during geomagnetically disturbed conditions. The results of such an investigation are presented in Figure 2. A superposed epoch analysis has been used to analyze average values of *AE* and *Dst* indices as a function of the time relative to the times of all 87 TILR events in Figures 2a and 2b, respectively. As suggested by Figure 1, the events measured in the Northern and Southern Hemispheres may be rather different; i.e., we performed the analysis for each hemisphere separately. The results obtained for the Northern Hemisphere are shown by the red curve, while the results obtained for the Southern Hemisphere are shown by the blue curve. It can be seen that there is no particularly striking variation of the analyzed geomagnetic indices at the times of the events. There may be a slight decrease of the *AE* index and a corresponding increase of the *Dst* index at the times of the events for the events observed both in the Northern Hemisphere and in the Southern Hemisphere, but given the overall variability of the dependence, this is far from significant.

Geographic locations where the TILR events were observed are shown in Figure 3. It is found that the events are observed only in a narrow longitudinal sector of Europe and western Africa; i.e., only this part of the world map is plotted. The spatial extent of the events observed in the Northern Hemisphere is shown by the thick solid red curves, and the spatial extent of the events observed in the Southern Hemisphere is shown by the thick solid blue curves. The thin red and blue curves show the trajectories of the DEMETER spacecraft during the half-orbits when the events were observed in the Northern and Southern Hemispheres, respectively. The thick black cross in the Northern Hemisphere shows the location of the GQD/GBZ VLF transmitter in Anthorn, Great Britain (22.1/19.6 kHz, $L \approx 2.40$), which approximately corresponds to the center of the area where the events are observed in the Northern Hemisphere. The thick black cross in the Southern Hemisphere shows the location of the geomagnetically conjugated point, and the black curve shows the projection of the corresponding magnetic field line. It can be seen that the events in the Southern

Hemisphere are not observed exactly in the region magnetically conjugated to the region where the events are observed in the Northern Hemisphere, but they are slightly shifted to lower magnetic latitudes. Further, while DEMETER nighttime half-orbits in this region roughly follow the magnetic meridian, the half-orbits where the events were observed in the Southern Hemisphere are still slightly westward from the half-orbits where the events were observed in the Northern Hemisphere.

The frequency spectra of the TILR events are analyzed in Figure 4a. An average frequency spectrum calculated over all the 87 identified events is shown. We note that the averaging was done in logarithm of the power spectral density, which allows to efficiently suppress occasional time intervals with extremely high intensity (e.g., the aforementioned spherics and whistlers). Again, the red curve corresponds to the events observed in the Northern Hemisphere and the blue curve corresponds to the events observed in the Southern Hemisphere. The vertical dashed lines mark the frequencies of individual peaks identified in the spectra at
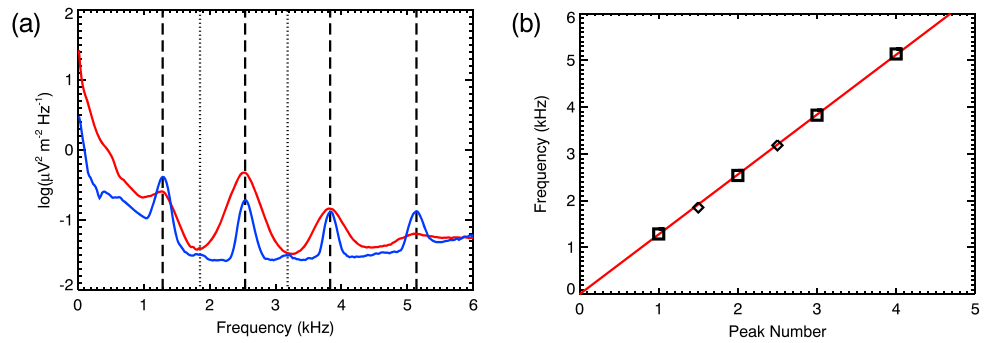
Figure 4. (a) Average frequency spectrum calculated over all 87 identified events. The averaging was done in the logarithm of the power spectral density. The red and blue curves show the results obtained for the events observed in the Northern and Southern Hemispheres, respectively. The vertical dashed lines mark the frequencies of individual spectral peaks identified in the spectra. The vertical dotted lines mark the frequencies of two additional very weak spectral peaks observable for the events located in the Southern Hemisphere. (b) Frequencies of individual spectral peaks as a function of their respective order are shown by the square symbols. The solid red line corresponds to the best linear fit. Frequencies of the two additional very weak spectral peaks observable for the events located in the Southern Hemisphere are shown by the diamonds, demonstrating that they are located just in between the main spectral peaks.

about 1.3 kHz, 2.5 kHz, 3.8 kHz, and 5.1 kHz. It can be seen that the frequencies of the spectral peaks observed in the Northern and Southern Hemispheres are about the same. However, the frequency bandwidth of the lines forming the events observed in the Northern Hemisphere is typically larger than the bandwidth of the lines forming the events observed in the Southern Hemisphere, in agreement with the example events in Figure 1. Additionally, very weak spectral peaks in between of the main ones, at frequencies of about 1.9 kHz and 3.2 kHz, are seen for the Southern Hemisphere events and marked by the vertical dotted lines. Note that the intensity enhancement at frequencies of about 0.5 kHz is due to natural electromagnetic emissions propagating from larger radial distances which reflect at the $L = 0$ cutoff close to the proton cyclotron frequency [see, e.g., *Santolík et al.*, 2006], and it is not related to the TILR events.

The frequency spacing between the harmonically spaced spectral peaks can be determined using a linear fit of individual peak frequencies, as it is demonstrated in Figure 4b. The frequencies of the respective spectral peaks as a function of their order are shown by square symbols. The solid red line in Figure 4b then corresponds to the best linear fit of the square symbols. This allows us to determine the frequency spacing between consecutive spectral peaks to be equal to about 1.28 kHz. The diamond symbols correspond to the two additional very weak spectral peaks at frequencies of about 1.9 kHz and 3.2 kHz observable in Figure 4a for the events located in the Southern Hemisphere. These are found to be observed just in between the main spectral peaks
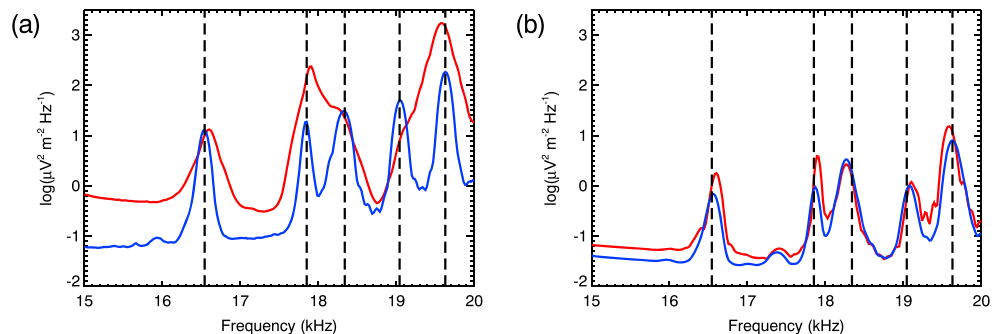
Figure 5. (a) Average frequency spectra in the frequency range between 15 and 20 kHz at the times of the events. The red and blue curves show the average spectra at the times of the events observed in the Northern and Southern Hemispheres, respectively. The black dashed vertical lines mark individual spectral peaks corresponding to VLF transmitter signals. (b) Average frequency spectra in the frequency range between 15 and 20 kHz measured in the geographical regions of the event occurrence. The data acquired during the entire duration of the mission were used, irrespectively whether they contain or not the analyzed events. The red and blue curves correspond to the results obtained in the geographical regions with the event occurrence in the Northern and Southern Hemispheres, respectively.

Figure 6. (a) Same as Figure 3. The black rectangle shows the latitude-longitude region where the events were observed. (b–f) Geographic maps of power spectral densities corresponding to individual transmitter peaks from Figure 5b. Approximately 100 Hz wide frequency ranges centered on the frequencies of spectral peaks were used in the calculation. The individual panels were obtained for central frequencies of 16.54 kHz, 17.85 kHz, 18.34 kHz, 19.04 kHz, and 19.63 kHz, respectively. 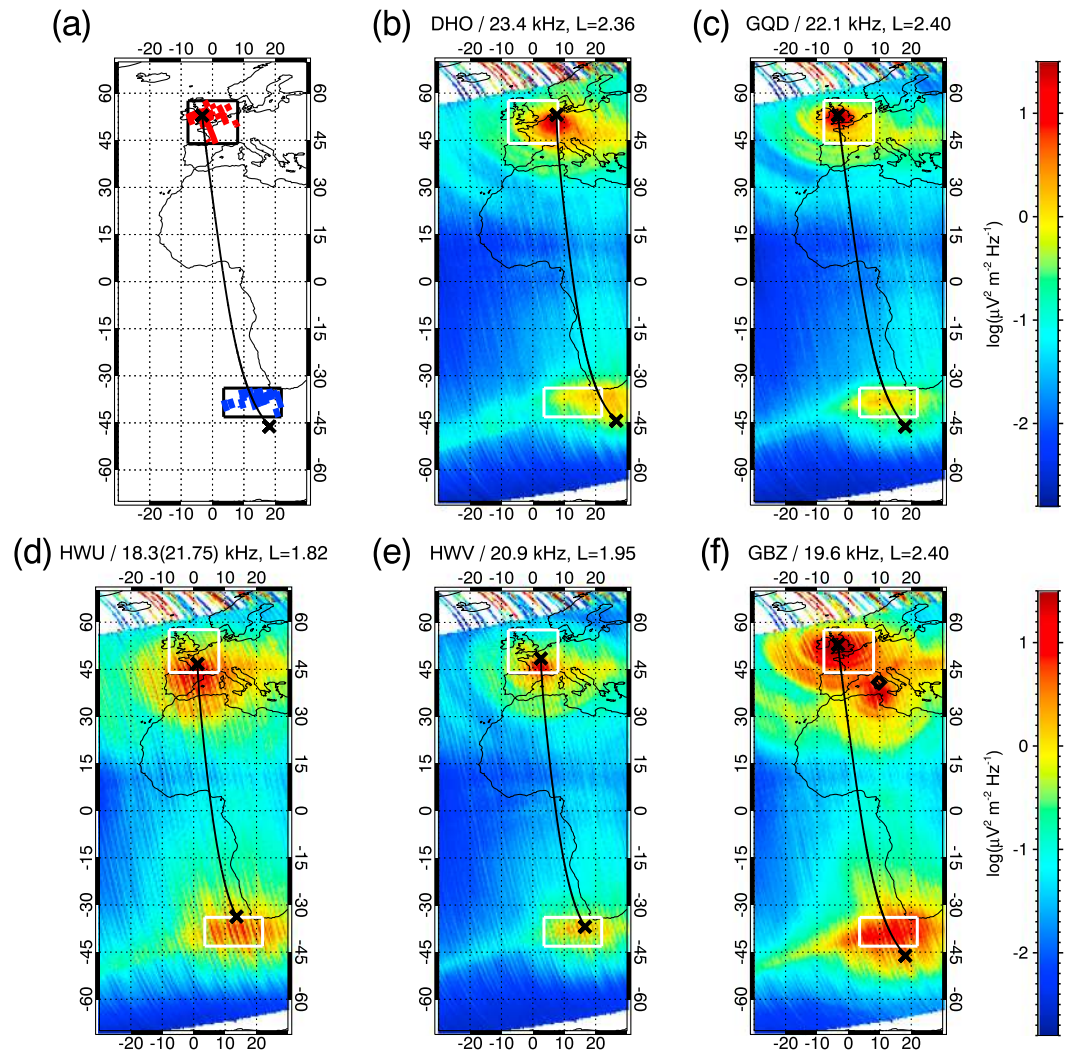The white rectangles mark the latitude-longitude region where the events were observed. The black crosses in the Northern and Southern Hemispheres correspond to the locations of VLF transmitters operating close to given central frequencies (or at frequencies aliased to given central frequencies) and their magnetic conjugates, respectively. The thick black curves show the projections of appropriate magnetic field lines. The transmitter code names, their frequencies, and L shells are given at the top. Figure 6f shows location of the ICV transmitter is shown by the black diamond.

(peak numbers 1.5 and 2.5, respectively). We further note that frequency-time spectrograms corresponding to TILR events generally exhibit increased power spectral densities of electric field fluctuations also at frequencies below 0.3 kHz (see Figure 1).

Figure 5a shows the average frequency spectra calculated over all the identified events in the same way as before, but this time the frequency range between 15 and 20 kHz is plotted, i.e., the frequency range relevant for the signals from VLF transmitters. Five spectral peaks at about 16.5 kHz, 17.9 kHz, 18.3 kHz, 19.0 kHz, and 19.6 kHz are identified. These are again marked by the black dashed vertical lines. Similarly as for the event spectral peaks, the frequency bandwidths of the transmitter signals observed in the Northern Hemisphere are noticeably larger than the frequency bandwidths of the transmitter signals observed in the Southern Hemisphere. This huge spectral broadening might be the reason that the transmitter signal at about 19.0 kHz is observable in the south, but not in the north, and it is a significantly different picture than a normal

Table 1. List of the VLF Transmitters Used in the Paper[a]

Code	Location	Latitude (deg)	Longitude (deg)	f (kHz)	Aliased f (kHz)	L Shell
DHO	Rhauderfehn, Germany	53.1	7.6	23.4	16.6	2.36
GQD	Anthorn, Great Britain	52.9	−3.3	22.1	17.9	2.40
HWU	Le Blanc, France	46.7	1.2	18.3	—	1.82
				21.75	18.25	
				22.6	17.4	
HWV	St Assise, France	48.5	2.6	20.9	19.1	1.95
GBZ	Anthorn, Great Britain	52.9	-3.3	19.6	—	2.40

[a]The code name, location, geographic longitude and latitude, the transmitter frequency, the aliased frequency taking into account the 40 kHz sampling of DEMETER VLF data, and the transmitter L shell are listed.

long-term average situation of the transmitter signal peaks shown in Figure 5b. This was obtained using all the DEMETER data measured in the areas of interest, i.e., in the latitude-longitude intervals corresponding to the locations of the event occurrence (shown by the black rectangle in Figure 6a). Specifically, under normal conditions, the frequency bandwidths of the transmitter signals observed in the Northern and Southern Hemispheres are approximately the same. Moreover, the long-term average signal intensities are lower than those observed at the times of the events. The long-term average spectra reveal also an additional minor spectral peak at the frequency of about 17.4 kHz not observable in the average frequency spectra at the time of the events.

It is in principle possible to determine individual VLF transmitters responsible for the spectral peaks in Figure 5. Knowing the frequency of a spectral peak, we can evaluate geographic maps of average power spectral densities of electric field fluctuations detected by DEMETER at that frequency. The geographic area where the detected intensity is the highest then provides us with a reasonable estimate of the transmitter location. Considering publicly available lists of existing VLF transmitters, and comparing their frequencies and locations with the frequency and location estimated from the DEMETER data, it is then possible to identify the exact transmitters involved. The geographic maps of long-term average power spectral densities corresponding to individual spectral peaks from Figure 5b are shown in Figures 6b–6f. They were constructed for approximately 100 Hz wide frequency ranges (i.e., five frequency bins of DEMETER VLF Survey mode measurements) centered at the frequencies of the spectral peaks from Figure 5a. They are presented in the order of increasing frequency; i.e., they were obtained for central frequencies of 16.54 kHz, 17.85 kHz, 18.34 kHz, 19.04 kHz, and 19.63 kHz, respectively. The black crosses in the Northern Hemisphere in Figures 6b–6f correspond to the locations of VLF transmitters operating close to given central frequencies (or at corresponding frequencies higher than 20 kHz which get close to given central frequencies due to aliasing) responsible for the observed intensity pattern. The black crosses in the Southern Hemisphere correspond to geomagnetically conjugated points, and the thick black curves show the projections of appropriate magnetic field lines. The transmitter in Figure 6b was identified as DHO transmitter in Rhauderfehn, Germany, which operates at 23.4 kHz, aliased to 16.6 kHz. The transmitter in Figure 6c was identified as GQD transmitter in Anthorn, Great Britain, which operates at 22.1 kHz, aliased to 17.9 kHz. The transmitter in Figure 6d was identified as HWU transmitter in Le Blanc, France. This transmitter operates at frequencies 18.3 kHz and 21.75 kHz (aliased to 18.25 kHz), which are both very close to the observed spectral peak at 18.34 kHz and not distinguishable in our analysis. Additionally, the HWU transmitter also operates at 22.6 kHz (aliased to 17.4 kHz), which results in the aforementioned minor spectral peak identifiable in the long-term average spectra in Figure 5b. The transmitter in Figure 6e was identified as HWV transmitter in St Assise, France, which operates at 20.9 kHz, aliased to 19.1 kHz. Finally, the transmitter in Figure 6f was identified as GBZ transmitter in Anthorn, Great Britain, which operates at 19.6 kHz. The transmitter code names, along with their frequencies and L shells, are shown at the tops of Figures 6b–6f. Figure 6a is the same as Figure 3; i.e., it shows the geographic locations where the events were observed by the DEMETER spacecraft. The respective longitude-latitude region is then shown by the black rectangle in Figure 6a and the white rectangles in Figures 6b–6f.

The used transmitters, along with their frequencies, geographic locations, and L shells, are listed in Table 1. It was compiled using the information provided in Table 1 of *Cohen et al.* [2012] and the Atmospheric Weather Electromagnetic System for Observation Modeling and Education (AWESOME) list compiled
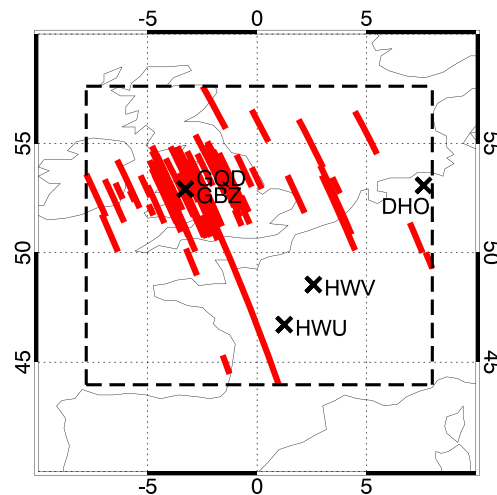
Figure 7. Enlarged geographic map of the region of interest. Spacecraft locations at the times when the events were observed are shown by the thick red curves. The black crosses show the locations of the five identified potentially relevant transmitters from Table 1, along with their call signs. The dashed black rectangle marks the latitude-longitude region where the events were observed.

by M. Cohen in 2009 (http:241//nova.stanford.edu/~vlf/ IHY_Test/TechDocs/AWESOME%20Transmitters.pdf). We note, however, that there are some minor disagreements between individual transmitter lists, which makes the exact identification of the transmitter properties and locations somewhat tricky. Nevertheless, these are not effectively needed for the performed analysis, and the rough identification of the involved transmitters is thus sufficient for the purpose of the presented paper.

It can be seen that all five potentially relevant transmitters are located in a spatially rather limited region of Great Britain, and northern parts of France and Germany, and their locations are in or very close to the region where the events are observed in the Northern Hemisphere. This is further demonstrated in Figure 7, which shows an enlarged geographic map of the region of interest. The thick red curves show the locations of the DEMETER spacecraft at the times when the events were observed. The locations of the five potentially relevant transmitters are shown by the black crosses and described by their respective code names. It can be seen that all the transmitters are located within the dashed rectangle, which marks the latitude-longitude region where the events were observed. However, the events occur noticeably more often just above the GQD/GBZ transmitters.

The situation in the Southern Hemisphere gets slightly more complicated. Due to the fact that the propagation generally cannot be considered as ideally ducted [*Clilverd et al.*, 2008; *Cohen and Inan*, 2012] and, moreover, there may be a significant scattering of the signal at density irregularities resulting in a change of wave normal angles [*Cohen and Inan*, 2012], the transmitter signals in the Southern Hemisphere are found to be detected not exactly in magnetically conjugated regions. Nevertheless, the regions with maximum transmitter signal intensities coincide rather well with the region where the events are observed in the Southern Hemisphere (marked by the black rectangle in Figure 6a and the white rectangles in Figures 6b–6f). We note that the ICV transmitter at Isola di Tavolara, Italy (40.9°N, 9.7°E, shown by the black diamond in Figure 6f), transmitting at 20.27 kHz (aliased to 19.73 kHz) is also located close to the geographic region of interest. Considering that the aliased frequency of the ICV transmitter is close to the frequency of the GBZ transmitter, its signal is readily identifiable in Figure 6f as an additional area of increased intensity. However, the ICV transmitter is located slightly apart from the locations of TILR events and the aforementioned relevant transmitters, and it does not seem to be involved in the TILR generation.

In order to further demonstrate that the generation of the TILR events is closely linked to the VLF transmitter signals, we employed a bicoherence analysis [*Lagoutte et al.*, 1989; *Graham et al.*, 2014]. This is possible, as high-resolution Burst mode data were available for (at least part of) seven events measured in the Northern Hemisphere and five events measured in the Southern Hemisphere. Basically, this allows us to investigate whether a three-wave interaction takes place between waves of frequencies f_1, f_2, and $f_1 + f_2$. Principally, the bicoherence analysis verifies whether the phases of the waves at given frequencies are related to each other or not. The resulting bicoherence values range from 0 (no relationship) to 1 (perfect relationship). The results are typically presented in a form of color-coded plots for all possible frequency combinations of f_1 and f_2. Further, given the symmetry reasons, we can limit the calculation only to a situation of $f_1 < f_2$. A single bicoherence plot is then obtained for each event with the Burst mode data available. Finally, we calculate an average bicoherence dependence for the events in the Northern Hemisphere and for the events in the Southern Hemisphere. These are shown in Figures 8a and 8b and 8c and 8d for the events observed in the Northern and Southern Hemispheres, respectively.
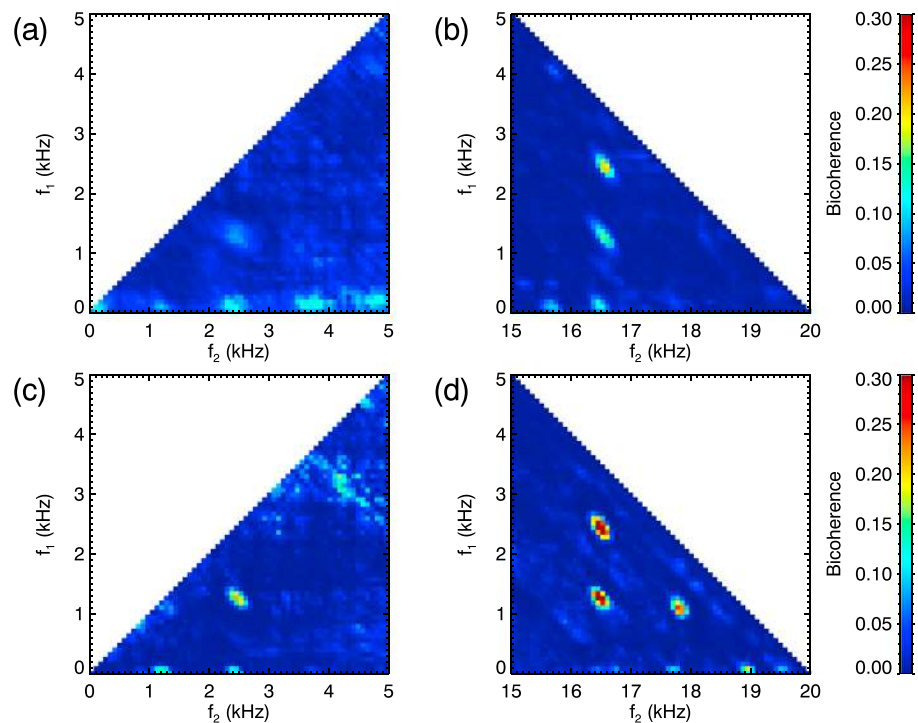
Figure 8. (a and b) Average bicoherence values calculated during the times of the events observed in the Northern Hemisphere. (c and d) Average bicoherence values calculated during the times of the events observed in the Southern Hemisphere. The values of bicoherence were calculated for each event separately and then averaged. The resulting average bicoherence values are color coded according to the scales on the right-hand side as a function of f_1 (ordinate) and f_2 (abscissa).

The average bicoherence values are color coded according to the scales on the right-hand side (the same for all plots) as a function of f_1 (ordinate) and f_2 (abscissa). The maximum frequency of the analysis is 20 kHz, corresponding to the Nyquist frequency with the 40 kHz waveform sampling. Note that we do not plot the bicoherence values for the frequency interval 5 kHz $< f_2 <$ 15 kHz, as no increased bicoherence values are observed in this frequency interval. It can be seen that the bicoherence values are not particularly high ($< \approx$ 0.3). This can be at least partly attributed to wideband whistler emissions occurring along with the events and interfering with the analysis. However, several frequencies with abnormally high bicoherence values can be identified. These increased bicoherence values occur at $f_1 \approx$ 1.3 kHz and $f_2 \approx$ 2.5 kHz (in particular for the events observed in the Southern Hemisphere, i.e., Figures 8c and 8d) and also at f_1 below 0.3 kHz and f_2 corresponding to harmonics of $\approx$ 1.3 kHz. This is not too surprising, and it indicates that individual harmonic lines forming the TILR events are phase locked. More interesting are the increased bicoherence values at $f_1 \approx$ 1.3 kHz and $f_2 \approx$ 16.5 kHz and $f_1 \approx$ 2.5 kHz and $f_2 \approx$ 16.5 kHz, indicating that signals at frequencies $\approx$ 16.5 kHz, $\approx$ 16.5 + 1.3 = 17.8 kHz, and $\approx$ 16.5 + 2.5 = 19.0 kHz are involved in the interaction. An additional area of increased bicoherence values is observed for the TILR events in the Southern Hemisphere at $f_1 \approx$ 1.2 kHz and $f_2 \approx$ 17.8 kHz, consistently indicating that signals at frequencies of $\approx$ 17.8 kHz and $\approx$ 17.8 + 1.2 = 19.0 kHz are involved. Considering the aliasing effect for frequencies above 20 kHz, the interacting signals revealed by the bicoherence analysis can be thus identified as coming from DHO ($\approx$ 23.4 kHz), GQD ($\approx$ 22.1 kHz), and HWV ($\approx$ 20.9 kHz) transmitters, respectively. It is important to notice that the frequency separations of the frequencies of these transmitters correspond to the observed base frequency of TILR events ($\approx$ 1.3 kHz).

Given that the generation of the events involves wave-wave interactions in the plasma medium, it is interesting to investigate whether they are accompanied by an enhanced precipitation of energetic electrons. We calculated a long-term average energy spectrum of precipitating electron flux using all DEMETER spacecraft data measured in the regions corresponding to the geographical coverage of half-orbits with the event occurrence. This was done separately for the events detected in the Northern and Southern Hemispheres. Then, we calculated an average energy spectrum of precipitating electron flux detected by DEMETER during the half-orbits when the events were observed, again separately for the events detected in the Northern and
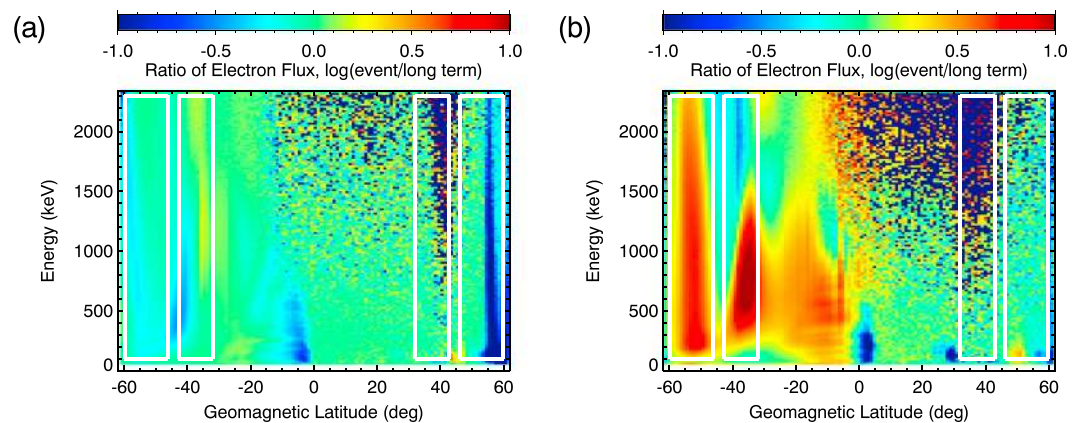
Figure 9. Ratios of energetic electron fluxes measured during half-orbits with the event occurrence and long-term energetic electron fluxes measured in the same regions. The results are color coded as a function of energy (ordinate) and geomagnetic latitude of the DEMETER spacecraft (abscissa). (a) Results obtained for the events observed in the Northern Hemisphere. (b) Results obtained for the events observed in the Southern Hemisphere. Only the data measured at geomagnetic longitudes corresponding to the half-orbits with the event occurrence were used at each geomagnetic latitude for the purpose of the long-term average calculation. The outer white rectangles (at larger geomagnetic latitudes) mark the geomagnetic latitudes of the events observed in the Northern Hemisphere and their magnetic conjugates. The inner white rectangles (at lower geomagnetic latitudes) mark the geomagnetic latitudes of the events observed in the Southern Hemisphere and their magnetic conjugates.

Southern Hemispheres. Finally, we calculated the ratio of the electron spectra detected during the half-orbits with the events and the long-term average electron spectra. These are plotted in Figures 9a and 9b as a function of the geomagnetic latitude for the events observed in the Northern and Southern Hemispheres, respectively. A logarithmic color scale is used; i.e., the plotted flux ratio effectively corresponds to the difference of respective logarithms. The white rectangles in the plots mark the geomagnetic latitudes of the event regions and the geomagnetic latitudes exactly opposite. The outer rectangles (at larger geomagnetic latitudes) correspond to the latitudes of the events observed in the Northern Hemisphere, while the inner rectangles (at lower geomagnetic latitudes) correspond to the latitudes of the events observed in the Southern Hemisphere. It can be seen that the electron fluxes measured in the Southern Hemisphere during the half-orbits when the events were observed in the Southern Hemisphere are significantly enhanced.

4. Discussion

The analyzed class of electromagnetic wave events has rather unique properties, which, by themselves, strongly suggest that the events are not completely natural, but their origin is related to man-made activity. Most importantly, while the DEMETER spacecraft sampling of the globe is in principle uniform, the events are observed in spatially rather limited regions. These are located close to Great Britain in the Northern Hemisphere and in the vicinity of the respective geomagnetically conjugated point in the Southern Hemisphere. This suggests that the events are generated by a process specific for a given magnetic meridian and L shell, which does not occur elsewhere. Additionally, the harmonically spaced frequency structure characteristic of the events is nearly exactly the same for all the observed events; i.e., the frequency separation between consecutive spectral peaks does not change from event to event. Should the events be generated naturally, one would expect the frequency separation to vary from event to event. Its constancy thus represents another piece of evidence for the events to be generated due to the man-made activity.

We suggest that the events are caused by electromagnetic signals from VLF transmitters penetrating through the ionosphere, which interact in the plasma environment and result in the formation of this new class of TILR wave events. Although we cannot support this by the available data, such interaction possibly takes place in the equatorial plane, which is a preferred region for wave-particle interactions [*Trakhtengerts and Rycroft*, 2008]. The larger-frequency bandwidth of individual lines forming the events observed in the Northern Hemisphere could be then possibly interpreted in the sense that the events observed in the Southern Hemisphere underwent a single passage through the equatorial interaction region, while the events observed in the Northern Hemisphere passed through the geomagnetic equator twice, once on the way to the south,

once on the way back to the north. The event generation due to the signals from VLF transmitters can naturally explain why they are preferentially observed in geographically limited regions. Additionally, such an explanation is consistent with the TILR events being observed exclusively during the night. During the day, the ionospheric attenuation is significantly larger [*Helliwell*, 1965], and the power of VLF transmitter signals leaking to the magnetosphere might thus be too low to result in the TILR formation. The event formation due to the VLF transmitters is also consistent with their occurrence principally independent of the geomagnetic activity characterized by *AE* and *Dst* indices, as it is the case also for the overall transmitter signal intensity [*Cohen and Inan*, 2012]. We note, however, that the event occurrence is, particularly in the Northern Hemisphere, related to the periods when the frequency bandwidths of the signals from VLF transmitters are significantly increased.

Two principal pieces of evidence that the event formation is related to the VLF transmitters in Europe were gathered. First, the locations where the events are observed by DEMETER are in agreement with the locations where the signals from VLF transmitters are observed, both in the Northern and Southern Hemispheres. Based on the geographic locations of the events and the transmitters, it appears that the transmitters operating in Great Britain should be particularly important for the event formation. However, a definite conclusion concerning the exact VLF transmitters involved cannot be made based on the geographic locations.

Second, and perhaps the most convincing piece of evidence for the events to be caused by VLF transmitters, which allows us—at least in principle—to determine the specific transmitters being involved, is a detailed analysis of the transmitter frequencies and a bicoherence analysis. A problematic point when performing this analysis is the limited sampling frequency of the DEMETER VLF measurements, which results in the frequency aliasing and an inability to distinguish between wave frequencies of $f_1 < 20$ kHz and very strong signals with $f_2 = 40$ kHz $- f_1$. We also note that the frequency differences between consecutive transmitter frequencies are often about the same, roughly corresponding to the base frequency of the analyzed events (≈ 1.3 kHz). This may actually be the principal reason that the events are formed, and it is further supported by the results of the bicoherence analysis. This analysis demonstrates that DHO, GQD, and GBZ transmitters operating at frequencies of 23.4 kHz, 22.1 kHz, and 19.6 kHz are involved in the interaction. This necessity of several powerful transmitters with close frequencies operating in a spatially limited area is likely the principal reason that the events are observed only in Europe and its magnetically conjugated region, and not in other parts of the world.

The generation mechanism of the events can be possibly similar to the formerly reported interaction between VLF transmitter signals and narrowband ELF emissions, which results in a formation of sideband structures around the transmitter signal [*Lagoutte et al.*, 1989; *Sotnikov et al.*, 1991; *Ohnami et al.*, 1993]. Such interaction was theoretically treated by *Tripathi and Patel* [1988] and *Trakhtengerts and Hayakawa* [1993]. The sidebands generated at the frequencies corresponding to the frequency difference of the input signals are likely electrostatic [*Inan and Bell*, 1985; *Tanaka et al.*, 1987], which seems consistent with the events not being identifiable in the DEMETER magnetic field data (not shown). Note, however, that DEMETER magnetic field data are significantly polluted by onboard spacecraft interferences, which substantially complicates the event identification. It should be noted that the very exact frequencies of the transmitter broadcasting are likely not that crucial in this regard, as the signals exhibit intrinsic bandwidths [*Cohen and Inan*, 2012], and their apparent frequencies can be further somewhat changed due to the Doppler shift [*Starks et al.*, 2009].

The increased power spectral densities at frequencies below 0.3 kHz observed at the times of the events are rather surprising. It is not clear at the moment how these are generated. They might be generated by the wave-wave interactions of VLF transmitter signals, in a similar manner as other spectral lines forming TILR events. Alternatively, they may correspond to an enhancement of a preexisting electrostatic plasma turbulence due to intense VLF signals propagating through the plasma medium. Finally, we cannot rule out the possibility that they are a manifestation of problems in the satellite electronics due to high amplitude signals measured at the times of TILR events, but the waveform of the signal does not show any saturation.

Concerning the influence of TILR events on the population of energetic electrons in the Van Allen radiation belts, we have demonstrated that the event formation is accompanied by enhanced energetic fluxes detected by DEMETER. Essentially, this corresponds to the fluxes of precipitating or nearly precipitating energetic electrons. It is curious to note that the increase of the energetic electron fluxes is observed only for half-orbits corresponding to the events observed in the Southern Hemisphere and only in the Southern Hemisphere. This phenomenon can be, however, likely explained by the presence of the South Atlantic Anomaly (SAA).

Specifically, due to the Earth's magnetic field not being a perfect dipole, energetic particles trapped in the radiation belts are more likely to precipitate in the region of the SAA than elsewhere. In other words, the loss cone in this region is larger, and the particles trapped in other magnetic meridians (outside the bounce loss cone) can get inside the loss cone at magnetic longitudes of SAA (drift loss cone). Considering the shape of DEMETER half-orbits shown in Figure 3, it can be seen that the half-orbits with events observed in the Southern Hemisphere (blue) are shifted noticeably to the west as compared to the half-orbits with the events observed in the Northern Hemisphere. Although this is a direct consequence of the specific DEMETER orbit, it also means that the half-orbits with the events observed in the Southern Hemisphere are closer to the magnetic meridian of the SAA; i.e., one would generally expect larger energetic electron precipitation at these half-orbits. Should the event occurrence be accompanied by a decrease of pitch angles of a population of energetic electrons, they would then precipitate at these geomagnetic longitudes in the Southern Hemisphere.

It is also curious to note that the observed energetic electron precipitation related to TILR events spans over a wide energy range. This is different than a typical discrete-energy radiation belt electron precipitation due to VLF transmitters [*Sauvaud et al.*, 2008], and it indicates more complicated interactions in the equatorial region and/or a continuous distribution of wave normal angles.

5. Conclusions

We presented a detailed systematic analysis of specific electromagnetic wave events observed by the low-altitude DEMETER spacecraft, which are formed by intense emissions at well-defined discrete, harmonically spaced frequencies. The appropriate frequency spectra are typically formed by up to four spectral peaks at multiples of about 1.3 kHz. Additional weaker spectral peaks at 1.9 kHz and 3.2 kHz are occasionally present. Altogether, 87 such events were identified in the available DEMETER data (about 6 years). The events occurred exclusively during the night, and they did not show any clear relation to the *AE* and *Dst* geomagnetic activity indices. We showed that the events are strongly localized, occurring either close to Great Britain or in the vicinity of its geomagnetically conjugated point. It was found that the events observed in the Northern Hemisphere generally have larger-frequency bandwidths than those observed in the Southern Hemisphere. We demonstrated that the events are linked to the signals from VLF transmitters in Europe. The bicoherence analysis was employed to demonstrate the wave-wave interactions taking place. Finally, we showed that the occurrence of these TILR events is associated with a significantly increased electron precipitation. Our results demonstrate that powerful VLF transmitters can significantly influence the wave activity in a given magnetic meridian, generating new emissions and resulting in energetic electron precipitation over a wide energy range.

References

Baker, D. N., et al. (2014), An impenetrable barrier to ultrarelativistic electrons in the Van Allen radiation belts, *Nature*, *515*, 531–534, doi:10.1038/nature13956.

Bell, T. F., U. S. Inan, D. Piddyachiy, P. Kulkarni, and M. Parrot (2008), Effects of plasma density irregularities on the pitch angle scattering of radiation belt electrons by signals from ground based VLF transmitters, *Geophys. Res. Lett.*, *35*, L19103, doi:10.1029/2008GL034834.

Berthelier, J. J., et al. (2006), ICE, the electric field experiment on DEMETER, *Planet. Space Sci.*, *54*, 456–471.

Bezděková, B., F. Němec, M. Parrot, O. Santolík, and O. Kruparova (2015), Magnetospheric line radiation: 6.5 years of observations by the DEMETER spacecraft, *J. Geophys. Res. Space Physics*, *120*, 9442–9456, doi:10.1002/2015JA021246.

Clilverd, M. A., C. J. Rodger, R. Gamble, N. P. Meredith, M. Parrot, J.-J. Berthelier, and N. R. Thomson (2008), Ground-based transmitter signals observed from space: Ducted or nonducted?, *J. Geophys. Res.*, *113*, A04211, doi:10.1029/2007JA012602.

Cohen, M. B., and U. S. Inan (2012), Terrestrial VLF transmitter injection into the magnetosphere, *J. Geophys. Res.*, *117*, A08310, doi:10.1029/2012JA017992.

Cohen, M. B., N. G. Lehtinen, and U. S. Inan (2012), Models of ionospheric VLF absorption of powerful ground based transmitters, *Geophys. Res. Lett.*, *39*, L24101, doi:10.1029/2012GL054437.

Dudkin, F., V. Korepanov, D. Dudkin, V. Pilipenko, V. Pronenko, and S. Klimov (2015), Electric field of the power terrestrial sources observed by microsatellite Chibis-M in the Earth's ionosphere in the frequency range 1–60 Hz, *Geophys. Res. Lett.*, *42*, 5686–5693, doi:10.1002/2015GL064595.

Foster, J. C., P. J. Erickson, D. N. Baker, A. N. Jaynes, E. V. Mishin, J. F. Fennel, X. Li, M. G. Henderson, and S. G. Kanekal (2016), Observations of the impenetrable barrier, the plasmapause, and the VLF bubble during the 17 March 2015 storm, *J. Geophys. Res. Space Physics*, *121*, 5537–5548, doi:10.1002/2016JA022509.

Foust, F. R., U. S. Inan, T. Bell, and N. G. Lehtinen (2010), Quasi-electrostatic whistler mode wave excitation by linear scattering of EM whistler mode waves from magnetic field-aligned density irregularities, *J. Geophys. Res.*, *115*, A11310, doi:10.1029/2010JA015850.

Gamble, R. J., C. J. Rodger, M. A. Clilverd, J.-A. Sauvaud, N. R. Thomson, S. L. Stewart, R. J. McCormick, M. Parrot, and J.-J. Berthelier (2008), Radiation belt electron precipitation by man-made VLF transmissions, *J. Geophys. Res.*, *113*, A10211, doi:10.1029/2008JA013369.

Graf, K. L., U. S. Inan, D. Piddyachiy, P. Kulkarni, M. Parrot, and J. A. Sauvaud (2009), DEMETER observations of transmitter-induced precipitation of inner radiation belt electrons, *J. Geophys. Res.*, *114*, A07205, doi:10.1029/2008JA013949.

Graf, K. L., N. G. Lehtinen, M. Spasojevic, M. B. Cohen, R. A. Marshall, and U. S. Inan (2013), Analysis of experimentally validated trans-ionospheric attenuation estimates of VLF signals, *J. Geophys. Res. Space Physics*, *118*, 2708–2720, doi:10.1002/jgra.50228.

Graham, D. B., D. M. Malaspina, and I. H. Cairns (2014), Applying bicoherence analysis to spacecraft observations of Langmuir waves, *Geophys. Res. Lett.*, *41*, 1367–1374, doi:10.1002/2014GL059565.

Helliwell, R. A. (1965), *Whistlers and Related Ionospheric Phenomena*, Stanford Univ. Press, Stanford, Calif.

Inan, U. S., and T. F. Bell (1985), Spectral broadening of VLF transmitter signals observed on DE 1: A quasi-electrostatic phenomenon?, *J. Geophys. Res.*, *90*(A2), 1771–1775.

Inan, U. S., M. Golkowski, M. K. Casey, R. C. Moore, W. Peter, P. Kulkarni, P. Kossey, E. Kennedy, S. Meth, and P. Smit (2007), Subionospheric VLF observations of transmitter-induced precipitation of inner radiation belt electrons, *Geophys. Res. Lett.*, *34*, L02106, doi:10.1029/2006GL028494.

Korepanov, V. E., F. L. Dudkin, and V. A. Pronenko (2015), Observations of radiation from power lines in near-Earth space, *Geomagn. Aeron.*, *55*(5), 688–692.

Kulkarni, P., U. S. Inan, T. F. Bell, and J. Bortnik (2008), Precipitation signatures of ground-based VLF transmitters, *J. Geophys. Res.*, *113*, A07214, doi:10.1029/2007JA012569.

Lagoutte, D., F. Lefeuvre, and J. Hanasz (1989), Application of bicoherence analysis in study of wave interactions in space plasma, *J. Geophys. Res.*, *94*(A1), 435–442.

Molchanov, O. A., M. Parrot, M. M. Mogilevsky, and F. Lefeuvre (1991), A theory of PLHR emissions to explain the weekly variation of ELF data observed by a low-altitude satellite, *Ann. Geophys.*, *9*, 669–680.

Nunn, D., J. Manninen, T. Turunen, V. Trakhtengerts, and N. Erokhin (1999), On the nonlinear triggering of VLF emissions by power line harmonic radiation, *Ann. Geophys.*, *17*, 79–94.

Němec, F., O. Santolík, M. Parrot, and J. J. Berthelier (2006), Power line harmonic radiation (PLHR) observed by the DEMETER spacecraft, *J. Geophys. Res.*, *111*, A04308, doi:10.1029/2005JA011480.

Němec, F., O. Santolík, M. Parrot, and J. J. Berthelier (2007), Power line harmonic radiation: A systematic study using DEMETER spacecraft, *Adv. Space Res.*, *40*, 398–403.

Němec, F., O. Santolík, M. Parrot, and J. Bortnik (2008), Power line harmonic radiation observed by satellite: Properties and propagation through the ionosphere, *J. Geophys. Res.*, *113*, A08317, doi:10.1029/2008JA013184.

Němec, F., M. Parrot, O. Santolík, C. J. Rodger, M. J. Rycroft, M. Hayosh, D. Shklyar, and A. Demekhov (2009), Survey of magnetospheric line radiation events observed by the DEMETER spacecraft, *J. Geophys. Res.*, *114*, A05203, doi:10.1029/2008JA014016.

Němec, F., M. Parrot, and O. Santolík (2010), Influence of power line harmonic radiation on the VLF wave activity in the upper ionosphere: Is it capable to trigger new emissions?, *J. Geophys. Res.*, *115*, A11301, doi:10.1029/2010JA015718.

Němec, F., M. Parrot, and O. Santolík (2012), Detailed properties of magnetospheric line radiation events observed by the DEMETER spacecraft, *J. Geophys. Res.*, *117*, A05210, doi:10.1029/2012JA017517.

Němec, F., M. Parrot, and O. Santolík (2015), Power line harmonic radiation observed by the DEMETER spacecraft at 50/60 Hz and low harmonics, *J. Geophys. Res. Space Physics*, *120*, 8954–8967, doi:10.1002/2015JA021682.

Ohnami, S., M. Hayakawa, T. F. Bell, and T. Ondoh (1993), Nonlinear wave-wave interactions in the subauroral ionosphere on the basis of ISIS-2 satellite observations of Siple station VLF signals, *Geophys. Res. Lett.*, *20*(8), 739–742.

Park, C. G., and R. A. Helliwell (1978), Magnetospheric effects of power line radiation, *Science*, *200*, 727–730.

Park, C. G., and R. A. Helliwell (1981), Power line radiation in the magnetosphere, *Adv. Space Res.*, *1*, 423–437.

Park, C. G., and T. R. Miller (1979), Sunday decreases in magnetospheric VLF wave activity, *J. Geophys. Res.*, *84*, 943–950.

Parrot, M. (1991), Daily variations of ELF data observed by a low-altitude satellite, *Geophys. Res. Lett.*, *18*(6), 1039–1042.

Parrot, M., and F. Němec (2009), MLR events and associated triggered emissions observed by DEMETER, *Adv. Space Res.*, *44*, 979–986.

Parrot, M., et al. (2006), The magnetic field experiment IMSC and its data processing onboard DEMETER: Scientific objectives, description and first results, *Planet. Space Sci.*, *54*, 441–455.

Parrot, M., F. Němec, and O. Santolík (2014), Statistical analysis of VLF radio emissions triggered by power line harmonic radiation and observed by the low-altitude satellite DEMETER, *J. Geophys. Res. Space Physics*, *119*, 5744–5754, doi:10.1002/2014JA020139.

Parrot, M., et al. (2015), Unexpected very low frequency (VLF) radio events recorded by the ionospheric satellite DEMETER, *Surv. Geophys.*, *36*, 483–511, doi:10.1007/s10712-015-9315-5.

Rodger, C. J., M. A. Clilverd, K. H. Yearby, and A. J. Smith (1999), Magnetospheric line radiation observations at Halley, Antarctica, *J. Geophys. Res.*, *104*(A8), 17,441–17,447.

Rodger, C. J., M. A. Clilverd, K. H. Yearby, and A. J. Smith (2000a), Temporal properties of magnetospheric line radiation, *J. Geophys. Res.*, *105*(A1), 329–336.

Rodger, C. J., M. A. Clilverd, K. H. Yearby, and A. J. Smith (2000b), Is magnetospheric line radiation man-made?, *J. Geophys. Res.*, *105*, 15,981–15,990.

Santolík, O., F. Němec, M. Parrot, D. Lagoutte, L. Madrias, and J. J. Berthelier (2006), Analysis methods for multi-component wave measurements on board the DEMETER spacecraft, *Planet. Space Sci.*, *54*, 512–527.

Sauvaud, J. A., T. Moreau, R. Maggiolo, J.-P. Treilhou, C. Jacquey, A. Cros, J. Coutelier, J. Rouzaud, E. Penou, and M. Gangloff (2006), High-energy electron detection onboard DEMETER: The IDP spectrometer, description and first results on the inner belt, *Planet. Space Sci.*, *54*, 502–511, doi:10.1016/j.pss.2005.10.019.

Sauvaud, J.-A., R. Maggiolo, C. Jacquey, M. Parrot, J.-J. Berthelier, R. J. Gamble, and C. J. Rodger (2008), Radiation belt electron precipitation due to VLF transmitters: Satellite observations, *Geophys. Res. Lett.*, *35*, L09101, doi:10.1029/2008GL033194.

Shao, X., B. Eliasson, A. S. Sharma, G. Milikh, and K. Papadopoulos (2012), Attenuation of whistler waves through conversion to lower hybrid waves in the low-altitude ionosphere, *J. Geophys. Res.*, *117*, A04311, doi:10.1029/2011JA017339.

Sotnikov, V. I., V. Fiala, F. Lefeuvre, and D. Lagoutte (1991), Excitation of sidebands due to nonlinear coupling between a VLF transmitter signal and a natural ELF emission, *J. Geophys. Res.*, *96*(A7), 11,363–11,369.

Starks, M. J., R. A. Quinn, G. P. Ginet, J. M. Albert, G. S. Sales, B. W. Reinisch, and P. Song (2008), Illumination of the plasmasphere by terrestrial very low frequency transmitters: Model validation, *J. Geophys. Res. Space Physics*, *113*, A09320, doi:10.1029/2008JA013112.

Starks, M. J., T. F. Bell, R. A. Quinn, U. S. Inan, D. Piddyachiy, and M. Parrot (2009), Modeling of Doppler-shifted terrestrial VLF transmitter signals observed by DEMETER, *Geophys. Res. Lett.*, *36*, L12103, doi:10.1029/2009GL038511.

Tanaka, Y., D. Lagoutte, M. Hayakawa, F. Lefeuvre, and S. Tajima (1987), Spectral broadening of VLF transmitter signals and sideband structure observed on Aureol 3 satellite at middle latitudes, *J. Geophys. Res.*, *92*(A7), 7551–7559.

Tao, X., J. Bortnik, and M. Friedrich (2010), Variance of transionospheric VLF wave power absorption, *J. Geophys. Res.*, *115*, A07303, doi:10.1029/2009JA015115.

Trakhtengerts, V. Y., and M. Hayakawa (1993), A wave-wave interaction in whistler frequency range in space plasma, *J. Geophys. Res.*, *98*(A11), 19,205–19,217.

Trakhtengerts, V. Y., and M. J. Rycroft (2008), *Whistler and Alfvén Mode Cyclotron Masers in Space*, 354 pp., Cambridge Univ. Press, Cambridge, U. K.

Tripathi, V. K., and V. L. Patel (1988), On the possibility of beat excitation of whistler sidebands in the magnetosphere via ponderomotive force, *Geophys. Res. Lett.*, *15*(11), 1299–1302.